

Yuwang LIU, Dongqi WANG, Shangkui YANG, Jinguo LIU, Guangbo HAO

Design and experimental study of a passive power-source-free stiffness-self-adjustable mechanism

© The Author(s) 2021. This article is published with open access at link.springer.com and journal.hep.com.cn

Abstract Passive variable stiffness joints have unique advantages over active variable stiffness joints and are currently eliciting increased attention. Existing passive variable stiffness joints rely mainly on sensors and special control algorithms, resulting in a bandwidth-limited response speed of the joint. We propose a new passive power-source-free stiffness-self-adjustable mechanism that can be used as the elbow joint of a robot arm. The new mechanism does not require special stiffness regulating motors or sensors and can realize large-range self-adaptive adjustment of stiffness in a purely mechanical manner. The variable stiffness mechanism can automatically adjust joint stiffness in accordance with the magnitude of the payload, and this adjustment is a successful imitation of the stiffness adjustment characteristics of the human elbow. The response speed is high because sensors and control algorithms are not needed. The variable stiffness principle is explained, and the design of the variable stiffness mechanism is analyzed. A prototype is fabricated, and the associated hardware is set up to validate the analytical stiffness model and design experimentally.

Keywords variable stiffness mechanism, stiffness self-regulation, bionic robot, modeling

Received April 21, 2020; accepted August 3, 2020

Yuwang LIU (✉), Dongqi WANG, Shangkui YANG, Jinguo LIU, Guangbo HAO (✉)

State Key Laboratory of Robotics, Shenyang Institute of Automation, Chinese Academy of Sciences, Shenyang 110016, China; Institutes for Robotics and Intelligent Manufacturing, Chinese Academy of Sciences, Shenyang 110169, China
E-mails: liuyuwang@sia.cn; G.Hao@ucc.ie

Guangbo HAO
School of Engineering-Electrical and Electronic Engineering, University College Cork, Cork, Ireland

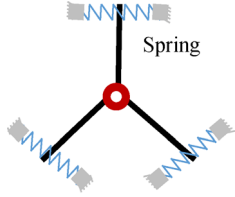
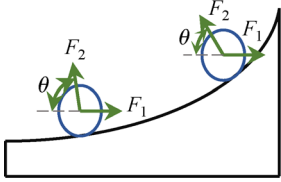
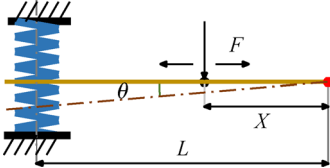
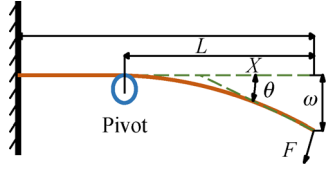
1 Introduction

Even in traditional industrial production, robots are no longer limited to structured environments; they have gradually become free of closed operating spaces by cooperating with humans and working with them in unstructured environments. Traditional industrial robots with high-stiffness joints usually excel in precision positioning and anti-disturbance but lack shock buffering and energy absorption functions. When directly used in cooperative and unstructured environments, such robots can easily collide with the surrounding objects and people; the robot body may become damaged by the strong collision, and the surrounding users may suffer from fatal injuries [1].

The use of flexible joints in robots is an effective approach to resolve the safety problems inherent to the process of human-machine cooperation in unstructured environments. The German Aerospace Center proposed the concept of active variable stiffness and successfully applied it to a KUKA robot [2]. This method uses an algorithm to simulate an elastic element that does not actually exist in the joint, thus making the joint actively flexible. The disadvantages are high energy consumption, severe impacts, and inability to store energy effectively. In addition, this method requires a complex sensor system to detect external information, and the real-time response capability of joint stiffness variation is limited due to the constraint in system bandwidth. The slow response leads to a high probability of non-compliant cooperation and collisions in unstructured environments.

The concept of passive variable stiffness was proposed to address the key issues of active variable stiffness [3–5]. In this concept, a self-adjustable mechanism (based on the elastic element) is added to the joint to change its stiffness. Compared with joints with active variable stiffness, those with passive variable stiffness have lower energy consumption, easier control, and faster response [6]; thus, they have gradually elicited increasing attention. Several typical passive variable stiffness joints are compared in Table 1

Table 1 Typical passive variable stiffness joints

Actuator	Schematic	Mode	Adjustment motor	Advantage	Disadvantage
SEA [7]		Modification of the output torque of the driving motor	No	Good impact resistance and energy storage	Low response speed
FSJ [8]		Combination of springs and curved surfaces	Yes	Diverse structure and small joint size	High energy consumption
Compact-VSA [9]		Adjustment of the effective length of the arm	Yes	Large stiffness variation	Complex structure
LVSJ [10]		Modification of the effective length of the leaf spring	Yes	Simple structure and easy control	Small stiffness variation

Abbreviation. SEA: Serial elastic actuator; FSJ: Floating spring joint; VSL: Variable stiffness joint; LVSJ: Low-cost variable stiffness joint.

[7–10].

The core components of several passive variable stiffness robots [7] (e.g., DOMO [11], Wendy [12], and cCub [13]) are serial elastic actuators (SEAs), with each having one or more springs with constant stiffness. An SEA is usually located at the output end of the joint and designed coaxially and serially with the driving motor of the joint. When the joint rotates, the torque of the joint's driving motor is controlled by sensing the output torque and spring deformation, thereby allowing the adjustment of joint stiffness. In passive variable stiffness joints, an elastic element is arranged inside the joint to improve the impact resistance and energy storage considerably. However, the demand on the sensor's capability to collect required information (e.g., displacement and force) is high, and the response speed is limited by the bandwidth.

In conjunction with linear springs and curved surfaces, joints such as RotWWC-VSA [14], AMASC [15], QA-Joint [16], FSJ [8], BAVS [17], and VS-Joint [18] can produce nonlinear variable stiffness characteristics. The stiffness of the joint is adjusted by changing the spring preloading through a special motor. The structure of this type is diverse, and the size of the joint is small. However,

the loading force is directly against the stiffness adjustment force because the direction of the force needed to change the joint stiffness is consistent with the direction of the spring deformation force; as a result, the energy consumption is high.

Joints such as AWAS-I, AWAS-II [19], compact-VSA [9], HVSA [20], vsaUT-II [21] MACCEPA [22], and MACCEPA 2.0 [23] use the lever principle to achieve stiffness adjustment. The joint stiffness varies with the change in the effective length of the force arm. The loading force is perpendicular to the stiffness adjustment force because the change in the direction of the force arm length is perpendicular to the direction of the elastic element reaction force. This type of design does not lead to direct confrontation, consumes relatively low energy, and requires only a small-sized special motor for stiffness adjustment. Through an appropriate structural design, this method can achieve large-range stiffness adjustment from zero to infinity at the cost of a complex structure.

The variable-stiffness joints designed in Refs. [24,25] and MeRIA [26], VsaMGR [27], VSJ [28], VSR-Joint [29], VSA-AP [30], and LVSJ [10] change stiffness by changing the effective length of the leaf spring (as a

cantilever beam). Given that the change in the direction of the leaf spring length is perpendicular to the direction of the reaction force of the elastic element, minimal energy is consumed, and the size of the special motor required is small. However, this method cannot achieve zero stiffness nor a wide range of stiffness change.

In summary, passive variable-stiffness joints have two main forms. The first form requires a special stiffness-regulating motor (or two parameter-equivalent motors whose coupling is used to achieve joint actuation and stiffness control). In this form, special sensors are installed to measure the loading information and provide feedback to the control unit for regulating stiffness. One or two special motors can be used to adjust stiffness. The majority of existing variable-stiffness joints adopt this form to adjust stiffness. However, the need for additional components not only increases the joint's size and weight but also results in joint complexity. The second form does not require a special stiffness-regulating motor but is equipped with a special sensor to measure the loading information and feed information back to the control unit. Stiffness-adjustable joints, such as those used in DOMO [7], can be obtained by controlling the torque of a driving motor. The resulting stiffness is linear and has a limited adjustment range because the core variable-stiffness component consists of springs with constant stiffness. The two forms of joints have low joint response speed and low system reliability due to the use of sensors and special control algorithms.

On the basis of these advancements, we present a new type of passive power-source-free stiffness-self-adjustable mechanism for use as the elbow joint of a robot arm. This new design does not require special stiffness-regulating motors, sensors, or control algorithms and can realize a large range of self-adaptive stiffness adjustment in a purely mechanical manner. No control algorithm is needed because the joint stiffness is adjusted based on the purely mechanical structure, and the joint's response speed is effectively guaranteed. The proposed design is different from the compact-VSA [19] shown in Table 1 in two ways. The first difference is that the proposed design passively changes stiffness by using force feedback, whereas VSA uses a drive motor to control stiffness actively. The second difference is that the proposed design adopts a different leverage principle.

The rest of the paper is organized as follows. Section 2 presents the imitation of the stiffness adjustment of human elbow joints and the design principle of the proposed passive power-source-free stiffness-self-adjustable mechanism. Section 3 introduces the mechanism's design details. Section 4 presents a theoretical analysis of the proposed passive power-source-free stiffness-self-adjustable mechanism, and Section 5 shows the experimental investigation and discussions of the stiffness calculation errors. Section 6 provides the conclusions.

2 Principle of the stiffness-self-adjustable mechanism

2.1 Design principle determination

From a biological perspective, human arm joints are variable-stiffness joints, among which the elbow joint has the most apparent variable stiffness characteristic [31,32]. When the front arm is naturally relaxed, the elbow is flexible with small joint stiffness, which can effectively reduce possible sudden impacts on the arm for protection. When the front arm is lifted up, the muscles inside the arm contract, and the elbow joint becomes stiff with large joint stiffness. When bearing different payloads in the lifting-up position, the self-adaptive elbow joint can allow for a wide range of effective stiffness adjustment. When the weight is large, the stiffness of the elbow joint is also large and vice versa. This study investigates the lifting-up position for stiffness self-adjustment.

On the basis of the characteristics of the human arm, a new passive power-source-free stiffness-self-adjustable mechanism for the elbow joint of a robot arm is developed in this study, as shown in Fig. 1. The main components of the passive power-source-free stiffness-self-adjustable mechanism include a stiffness-self-adjustable module and a double-stage four-linkage mechanism. The stiffness-self-adjustable module is embedded into the elbow joint to realize stiffness adjustment, and the double-stage four-linkage mechanism is arranged in the front arm to transfer information on the loading weight on the hand. Thus, the stiffness of the joint is automatically adjusted in accordance with the weight of objects. When an object is heavy, the stiffness of the elbow joint is large and vice versa. The stiffness adjustment characteristics of a human arm are therefore simulated effectively. The stiffness regulation of the stiffness-self-adjustable module and the feedback of the loading information do not require a power source or a sensor and are fully realized through a mechanical mechanism design.

2.2 Principle and parameters of the stiffness-self-adjustable module

The stiffness-self-adjustable module uses the lever principle, as shown in Fig. 2, in which point A is the contact point between the lever and spring, point B is the point of external force that can move along rod \overline{AC} , and point C is the fulcrum of the lever. Force F_B generated by the regulation module of external force action is applied to point B . In addition, F_A is the elastic resistance generated by the spring due to the rotation of the lever around point C when F_B is applied to point B . According to the well-known stiffness formula $k(\theta) = d\tau/d\theta$ (where τ is the equivalent torque exerted on the joint), the ratio of L to L_0 decreases when point B moves toward point C . Therefore,

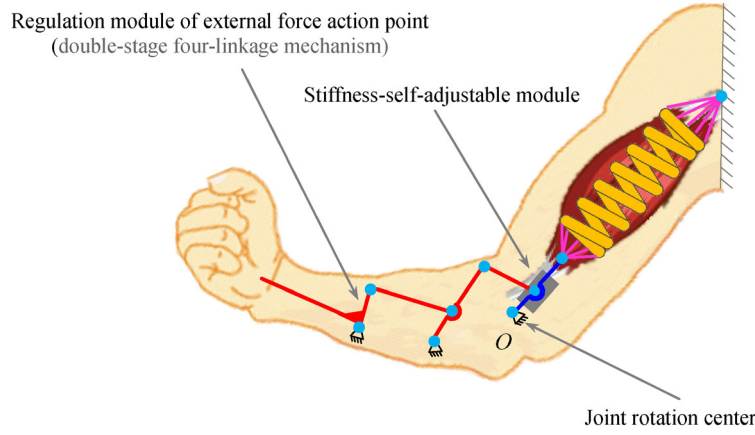


Fig. 1 Passive power-source-free stiffness-self-adjustable mechanism for elbow joint.

θ becomes small for the same F_B , and the joint stiffness increases. Similarly, the ratio of L to L_0 increases, θ increases, and the joint stiffness decreases when point B moves toward point A . Point C is not mobile in Fig. 2 to simplify the principle explanation, which is not the case in the final design.

2.3 Principle and parameters of the regulation module of the external force action point

The main function of the regulation mechanism of external force action point is realized by using a double-stage four-linkage mechanism, as shown in Fig. 3, to make full use of the space in the front arm and transform the gravity information of the weight at the end of the arm into a change in the displacement of point B on the lever (Fig. 1). F_1 is the gravity of the weight loaded at the end of the manipulator (initially in the horizontal/lifting-up position) defined at end point J , which is converted into force F_3 applied at point B through the double-stage four-linkage mechanism. F_3 balances the spring force generated by

the movement of point B . Notably, due to two-force rod l_6 , the direction of F_3 is along the axis of the two-force rod, and the direction of the force of the other two-force bar is determined based on the same reason, as shown in Fig. 3. Therefore, the following equation can be obtained.

$$k_2 \Delta x - F_3 \cos \varphi_3 = 0,$$

where k_2 is the stiffness of the torsion spring as shown in Fig. 3.

The larger F_1 is, the farther point B is from its initial position. The smaller F_1 is, the closer point B is to its initial position. When F_1 increases, with the translation of point B , the ratio of L to L_0 decreases, and the joint stiffness increases. When F_1 is small, the ratio of L to L_0 increases, and the stiffness of the joint decreases. This analysis indicates that the larger F_1 is, the higher the stiffness of the joint is; the smaller F_1 is, the lower the stiffness of the joint is. This condition can allow the stiffness of the elbow joint to be automatically adjustable in accordance with the weight of gravity at the end of the arm.

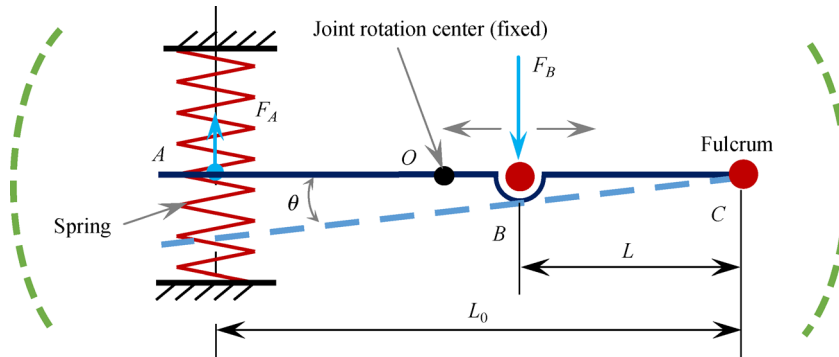


Fig. 2 Illustration of the principle of the stiffness-self-adjustable module.

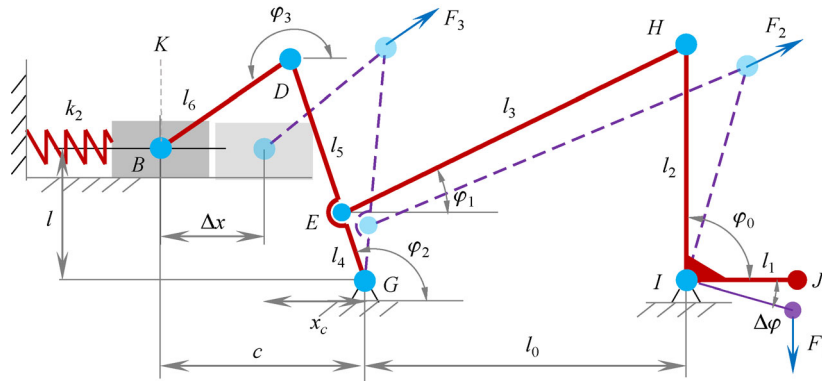


Fig. 3 Schematic of the regulation module of the external force point.

3 Mechanism design

On the basis of the design principle presented in Section 2, a stiffness-self-adjustable mechanism for the elbow joint is designed, as shown in Fig. 4. The passive power-source-free stiffness-self-adjustable mechanism is mainly composed of two parts: The stiffness-self-adjustable module and the regulation module of the external force action point.

The stiffness-self-adjustable module is shown in Fig. 4(a). A synchronous belt is fixed at the end of the lever, and a synchronous pulley is mounted on the column through a bearing. The synchronous belt meshes with the synchronous pulley. One end of the torsion ring at the outer ring of the column is fixed to the synchronous pulley, and its other end is fixed to the outer shell of the joint. When the lever swings, the torsion spring deforms and produces resistance force. When the slider moves to the left end of the slot, the stiffness of the elbow joint is minimal; when the slider moves to the right end of the slot, the slider and point C coincide such that the stiffness of the joint

approaches infinity. The maximal relative rotation angle between the lower and connecting covers is controlled by the limit mechanism, thus preventing the elastic element from experiencing excessive/plastic deformation. The limit mechanism is realized by connecting the U-type groove on the connection cover and the U-type protruding on the lower cover. When the U-type protruding on the lower cover is rotated to the end of the U-type groove, no further relative rotation occurs. The relative rotation angle range is $[-12^\circ, +12^\circ]$ due to the constraints of the designed structure and internal dimensions.

The regulation module of the external force action point is shown in Fig. 4(b). When external force F_1 is applied at the end of the driving rod, the swinging of the driving rod eventually changes into a slider movement along the guide rail through a double-stage four-bar mechanism. The resulting spring force (from the stretch spring connected to the slider) balances external force F_1 . When external force F_1 is small, the displacement of the slider on the guide rail is small and vice versa. The double-stage four-bar mechanism is embedded into the front arm, which not

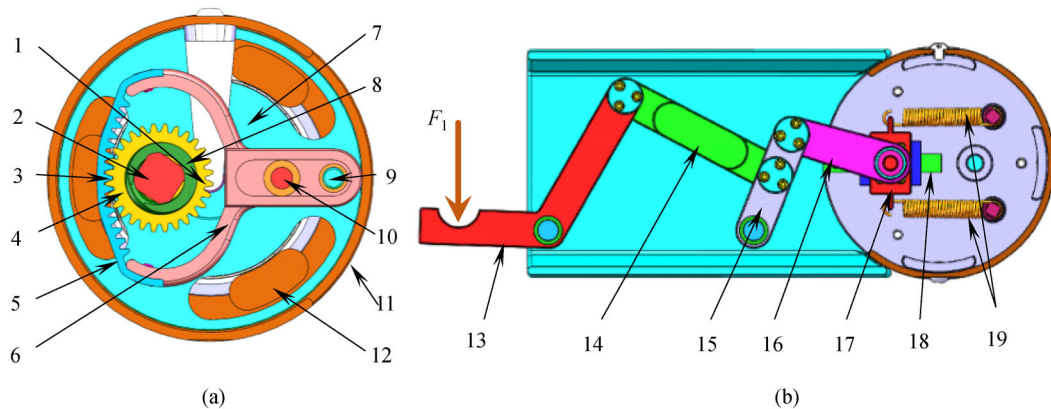


Fig. 4 3D model of the variable stiffness mechanism. (a) Stiffness-self-adjustable module using the lever principle; (b) regulation module of the external force action point. 1–Point O; 2–Pillar; 3–Point A; 4–Synchronous pulley; 5–Synchronous belt; 6–Lever; 7–Limit mechanism; 8–Torsion spring; 9–Connection cover (point C in principle diagram); 10–Slider (point B in principle diagram); 11–Lower cover; 12–Connection cover; 13–Driving rod; 14–Connecting rod 1; 15–Driven rod; 16–Connecting rod 2; 17–Slider; 18–Guide; 19–Stretch spring.

only reduces the footprint of the entire mechanism but also transfers the end force of the manipulator to the stiffness-self-adjustable module at the elbow joint.

An explosion diagram of the passive stiffness-self-adjustable mechanism is shown in Fig. 5. The mechanism is mainly composed of the regulation module of the external force action point, the stiffness-self-adjustable module, an upper cover, a lower cover, and a pressure cap.

The slider based on the regulation module of the external force action point is fixed to the upper cover, and the sliding part is connected with the double-stage four-linkage mechanism. One end of the lever of the stiffness-self-adjustable module is connected with the slider part of the regulation module of the external force action point, and its other end is fixed to the connecting cover. The bearing is fixed to the lower cover through the cap to prevent axial movement.

4 Stiffness theoretical analysis

4.1 Parameter determination of the double-stage four-linkage mechanism

As shown in Fig. 3, when rod l_1 , which is in direct contact with the terminal loading, swings downward, the double-stage four-linkage mechanism allows the slider to move horizontally to the right. Therefore, the double-stage four-linkage mechanism's parameter selection affects the performance of the elbow joint. The transmission efficiency will be low if the transmission angle ($\angle KBD$ and $\angle DEH$) is too small. We define $\Delta\varphi_{\max}$, which is the maximum rotation value of $\Delta\varphi$ (Fig. 3) during the slider movement from the initial position to the end position. If $\Delta\varphi_{\max}$ is too large, the performance of the joint will be adversely affected. Therefore, selecting reasonable rod parameters for minimizing $\Delta\varphi_{\max}$ is important.

The length of each rod is used as a design variable, which is included in the vector

$$\mathbf{X} = [x_1, x_2, x_3, x_4, x_5]^T = [l_2, l_3, l_4, l_5, l_6]^T. \quad (1)$$

The details of all relevant constraint functions are shown in Table 2 [33].

The objective of optimization is to minimize the angle $\Delta\varphi_{\max}$ of the driving rod when point B swings from the initial to the end position. Thus, the optimization function is established as

$$\begin{cases} \mathbf{X} = [x_1, x_2, x_3, x_4, x_5]^T, \\ \text{s.t. } g_i(\mathbf{X}) \leq 0 \quad (i = 1, 2, \dots, 17), \\ \min f(\mathbf{X}) = \min(\Delta\varphi_{\max}). \end{cases} \quad (2)$$

The optimized connecting rod length under the given initial value of each link is shown in Table 3. Angle $\Delta\varphi_{\max}$ changes from 14.7° to 12.91° , which means that the optimization effect is remarkable.

4.2 Stiffness model of the joint

A schematic analysis of the stiffness-self-adjustable module is shown in Fig. 6. The symbol definition is shown as follows:

- τ : Equivalent torque applied to the elbow joint;
- ϕ : Rotation angle of the elbow joint under the action of torque;
- θ_1 : Rotation angle of the torsion spring due to the applied force;
- θ_2 : Rotation angle of the lever around point B ;
- F' : Reaction force of the fulcrum;
- F : Component of F' that is tangent to the outer circle;
- F_2 : Reaction force of the synchronous belt and pulley;
- F'_2 : Corresponding reaction force of F_2 while rotating as shown by the red arrow, the direction of which is similar to that of F_2 ;
- F_0 : Component of F'_2 from the torsion spring that is perpendicular to PB ;
- K : Variable stiffness mechanism stiffness value;
- O : Center of rotation of the elbow joint;
- A : Contact point of the synchronous belt and pulley when the level is horizontal;
- B : Point of external force;
- C : Fulcrum of the lever;

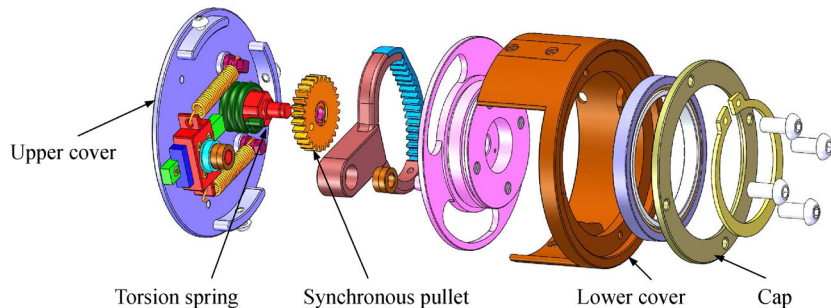


Fig. 5 Explosion diagram of the stiffness-self-adjustable mechanism.

Table 2 Derivation of the constraint functions of the double-stage four-linkage mechanism

Constraint	Expression	Constraint function
The transmission angle is not less than 60° [33]	$\begin{cases} \angle KBD \geq 60^\circ, \\ \angle DEH \geq 60^\circ. \end{cases}$	$\begin{cases} g_1(x) = \varphi_3 - 240^\circ, \\ g_2(x) = \arcsin \frac{l_0 - x_4 \sin \varphi_2}{x_5} - \frac{4\pi}{3}. \end{cases}$
Existence condition of the crank of the four-linkage mechanism [33]	$\begin{cases} l_4 + l_0 \leq l_2 + l_3, \\ l_3 + l_4 \leq l_0 + l_2, \\ l_2 + l_4 \leq l_0 + l_3, \\ l_5 - l_6 < l_0, \\ l_3 \geq l_4, \\ l_2 \geq l_4. \end{cases}$	$\begin{cases} g_3(x) = l_0 + x_3 - x_1 - x_2, \\ g_4(x) = x_2 + x_3 - x_1 - l_0, \\ g_5(x) = x_1 + x_3 - l_0 - x_2, \\ g_6(x) = x_4 - x_5 - l_0, \\ g_7(x) = x_3 - x_2, \\ g_8(x) = x_3 - x_1. \end{cases}$
Range of rod size ^{a)}	$\begin{cases} 0 \text{ mm} < l_2 \leq 56 \text{ mm}, \\ 60 \text{ mm} \leq l_3 \leq 120 \text{ mm}, \\ 24 \text{ mm} \leq l_4 \leq 50 \text{ mm}, \\ 35 \text{ mm} \leq l_5 \leq 50 \text{ mm}, \\ 35 \text{ mm} \leq l_6 \leq 40 \text{ mm}. \end{cases}$	$\begin{cases} g_9(x) = x_1 - 56, \\ g_{10}(x) = x_2 - 120, \\ g_{11}(x) = x_3 - 50, \\ g_{12}(x) = x_4 - 50, \\ g_{13}(x) = x_5 - 40, \\ g_{14}(x) = 60 - x_2, \\ g_{15}(x) = 24 - x_3, \\ g_{16}(x) = 35 - x_4, \\ g_{17}(x) = 35 - x_5. \end{cases}$

^{a)} According to the average size of the adult arm structure ratio.

Table 3 Comparison of the bar length before and after optimization

Link	Bar length/mm	
	Initial value	After optimization
l_2	56	56
l_3	60	66
l_4	28	24
l_5	40	40
l_6	50	40

P : Contact point of the synchronous belt and pulley while rotating;

Z : Fulcrum position when the level is horizontal;

Z' : Projection of C on AB ;

r : Radius of the synchronous pulley;

T : Torque value on the synchronous pulley;

R : Radius of the outer circle, the distance from the lever fulcrum to the center of rotation;

x_1 : Distance between A and B ;

x_2 : Distance between B and C ;

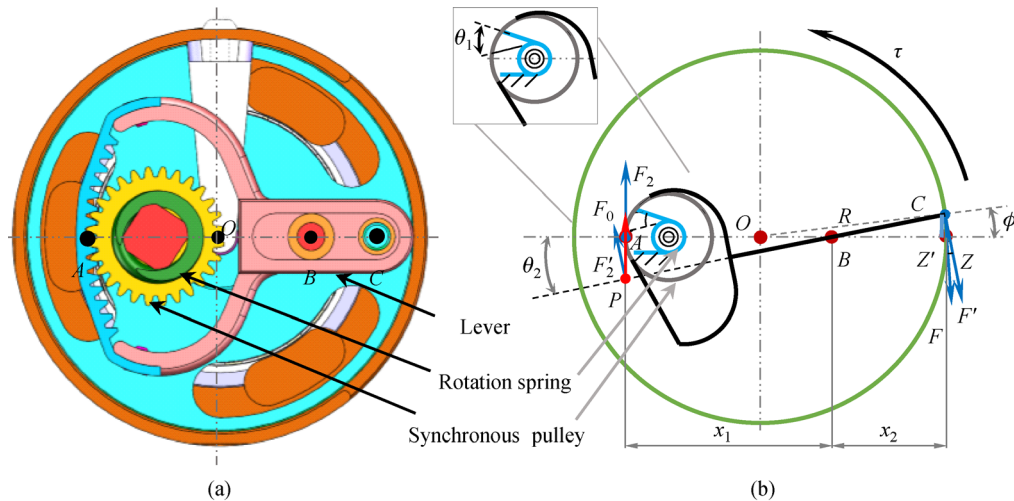


Fig. 6 Schematic of the stiffness-self-adjustable module. (a) Stiffness-self-adjustable module model and (b) stiffness-self-adjustable module schematic.

k_1 : Stiffness of the torsion spring.

The torque generated by the torsion spring deformation is $T = k_1\theta_1$. Given that the torsion spring is fixed on the synchronous pulley, the same torque is transmitted to the synchronous pulley.

$$T = F_2 r, \quad (3)$$

where r is the pitch radius of the timing pulley.

Considering that F_2 and F'_2 are along the same direction, according to the translation theorem of force, there is no added force if F_2 moves to point P .

Given that F_0 is the component of F_2 , by combining Eqs. (3) and (4), we obtain

$$F_0 = \frac{k_1 \theta_1 \cos \theta_2}{r}. \quad (4)$$

Point B is the pivot point of the lever; thus, according to the principle of leverage, we can achieve the following equation.

$$F' = F_0 \frac{\overline{PB}}{\overline{BC}}. \quad (5)$$

The arc length rotated by the synchronous pulley is approximately equal to the arc length rotated by the lever around point B point, that is, $x_1 \theta_2 \approx r \theta_1$ can be obtained with the arc length formula.

By using Eqs. (4) and (5), we derive

$$F' = k_1 \theta_2 \frac{x_1^2}{r^2 \overline{BC}}. \quad (6)$$

According to the theorem of arc length, $R\phi = x_2 \theta_2$. In consideration of Eq. (6), we derive

$$F' = k_1 \frac{x_1^2}{r^2 x_2 \overline{BC}} R\phi. \quad (7)$$

Given that $F = F'/\cos(\theta_2 - \phi)$, Eq. (7) is rewritten as

$$F = k_1 \frac{x_1^2 R \phi}{r^2 x_2 \overline{BC} \cos(\theta_2 - \phi)}. \quad (8)$$

The equivalent torque applied to the elbow joint is

$$\tau = FR = k_1 \frac{x_1^2 R^2 \phi}{r^2 x_2 \overline{BC} \cos(\theta_2 - \phi)}. \quad (9)$$

θ_2 is small because the angle of the joint rotation (ϕ) is small. Hence, Eq. (9) can be simplified as

$$\tau = k_1 \frac{x_1^2 R^2 \phi}{r^2 x_2^2}. \quad (10)$$

Joint stiffness is then obtained:

$$K = \frac{\tau}{\phi} = k_1 \frac{x_1^2 R^2}{r^2 x_2^2}, \quad (11)$$

where $L = x_1 + x_2$, which is a constant.

The stiffness-self-adjustable module parameters used as input conditions for subsequent analysis are $R = 34$ mm, $r = 14.33$ mm, and $L = 62.33$ mm.

With torsion spring stiffness k_1 and slider movement displacement x_1 , the trend of the joint stiffness variation is obtained using Eq. (11), as shown in Fig. 7.

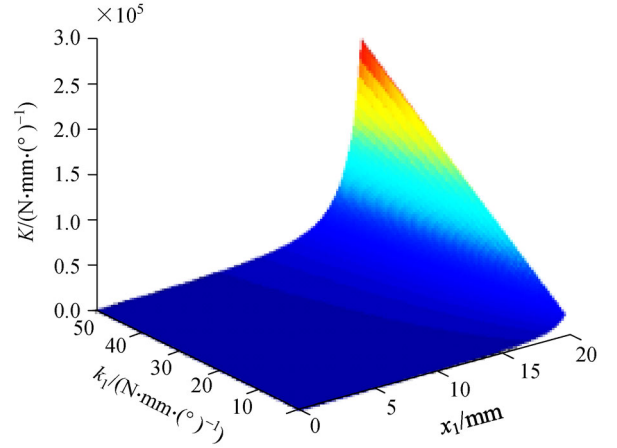


Fig. 7 Stiffness adjustment range of the stiffness-self-adjustable module.

When k_1 and R are constant, the change in joint stiffness becomes increasingly fast as x_1 increases. The stiffness of the joint can be adjusted within a large range within a small action range. When R and x_1 are constant, the relation between joint stiffness and torsion spring stiffness (k_1) is linear, and joint stiffness increases with the increase in torsion spring stiffness.

4.3 Force analysis of the double-stage four-linkage mechanism

In accordance with the regulation mechanism of the external force action point shown in Fig. 3, the relation between external force F_1 and the displacement of external force action point J can be obtained. The desired relationship between external force F_1 and the resulting self-adjustable joint stiffness can be obtained using the joint stiffness formula (Eq. (11)).

In accordance with the loading analysis of the double-stage four-linkage mechanism, the force-balance equations of the rods can be easily obtained as

$$\begin{cases} F_1 l_1 \cos(\Delta\varphi) = F_2 l_2 \cos\left(\varphi_0 - \Delta\varphi - \frac{\pi}{2} - \varphi_1\right), \\ F_2 l_4 \cos\left(\varphi_1 - \varphi_2 + \frac{\pi}{2}\right) = F_3 l_5 \cos\left(\varphi_3 - \varphi_2 - \frac{\pi}{2}\right), \\ F_3 \cos(\varphi_3 - \pi) = k_2 \Delta x, \end{cases} \quad (12)$$

where k_2 is the stiffness of the stretching spring in Fig. 6 and Δx is the displacement of the slider (motion on the initial position under no external loading).

Thus, we obtain

$$F_1 = \frac{l_2 l_5 k_2 \Delta x \cos\left(\varphi_3 - \varphi_2 - \frac{\pi}{2}\right) \cos\left(\varphi_0 - \Delta\varphi - \frac{\pi}{2} - \varphi_1\right)}{l_1 l_4 \cos(\varphi_3 - \pi) \cos\Delta\varphi \cos\left(\varphi_1 - \varphi_2 + \frac{\pi}{2}\right)}. \quad (13)$$

If we specify l_0 , l_2 , l_3 , and l_4 to represent the vectors of a closed vector loop (Fig. 3), the following vector equation in the double-stage four-linkage mechanism can be obtained:

$$\vec{l}_0 + \vec{l}_2 = \vec{l}_3 + \vec{l}_4. \quad (14)$$

We let the rotational angles be positive for the counter-clockwise direction with respect to the horizontal axis. Using the Euler formula, we derive

$$\begin{aligned} l_0 + l_2(\cos\varphi_0 + \sin\varphi_0) \\ = l_4(\cos\varphi_2 + \sin\varphi_2) + l_3(\cos\varphi_1 + \sin\varphi_1). \end{aligned} \quad (15)$$

The real or imaginary parts on both sides of Eq. (5) should be equal. By eliminating φ_1 , we obtain

$$\begin{aligned} l_3^2 = (l_2 \sin\varphi_0 - l_4 \sin\varphi_2)^2 \\ + (l_0 + l_2 \cos\varphi_0 - l_4 \cos\varphi_2)^2. \end{aligned} \quad (16)$$

Equation (16) can be rewritten in a trigonometric form as follows:

$$A \cos\varphi_2 + B \sin\varphi_2 + C = 0, \quad (17)$$

where $A = -l_0 - l_2 \cos\varphi_0$, $B = -l_2 \sin\varphi_0$, and $C = (l_4^2 - l_3^2 + A^2 + B^2)/(2l_4)$.

We can solve Eq. (17) for φ_2 as

$$\varphi_2 = 2 \arctan \frac{B - \sqrt{A^2 + B^2 - C^2}}{A - C}. \quad (18)$$

Similarly, φ_1 can be obtained as

$$\varphi_1 = 2 \arctan \frac{E + \sqrt{D^2 + E^2 - F^2}}{D - F}, \quad (19)$$

where $D = -l_0 - l_2 \sin\varphi_0$, $E = -l_2 \sin\varphi_0$, and $F = (l_3^2 - l_4^2 + D^2 + E^2)/(2l_4)$.

By using the same steps as above, we can construct another vector loop composed of l , x_c , l_5 , and l_6 to obtain the following result:

$$\sin\varphi_3 = \frac{l - l_5 \sin\varphi_2}{l_6}, \quad (20)$$

where x_c is the distance from the slider to the end position.

In summary, Eq. (20) is an expression of φ_3 with respect to φ_2 , Eq. (18) is an expression of φ_2 with respect to φ_0 , and Eq. (19) is an expression of φ_1 with respect to φ_0 .

When $\Delta\varphi$ is set as an independent variable and φ'_0 is defined as the deflection of φ_0 after rotating, the displacement Δx of the slider movement can be obtained by combining the result of $\varphi'_0 = \varphi_0 - \Delta\varphi$ and Eqs. (17)–(19), as follows:

$$\Delta x = c - x_c = c - l_5 \cos\varphi_2 - l_6 \cos\varphi_3, \quad (21)$$

where c is the distance between the initial and end positions of the slider.

By considering Eq. (13) and the results above (Eqs. (18)–(20)), we can obtain the relationship between F_1 and $\Delta\varphi$ or φ_0 . On the basis of Eq. (21), we can then obtain the relationship between F_1 and Δx . Given that $x_1 = \overline{AB}$ and point B is the slider moving point, the length of \overline{AB} is the distance between points A and B (B in the initial state) plus the displacement (Δx) of point B . Therefore, Eq. (11) can be revised to consider the effect of F_1 on joint stiffness.

Figure 8 shows the relation curve of joint stiffness K and gravity F_1 at the end of the manipulator. The different curves correspond to the torsion springs with different stiffness. As the external force increases, the slider gradually moves from the initial position to the end position, and the joint stiffness varies from a small value to infinity. In the case of the same external force, the greater the stiffness of the torsion spring is, the greater the stiffness of the joint is.

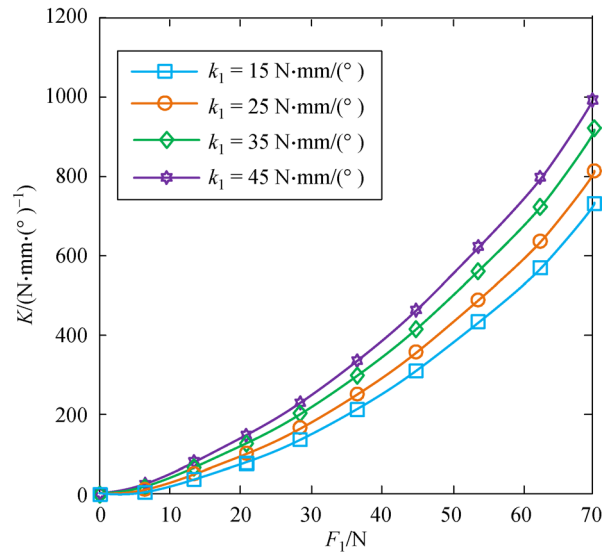


Fig. 8 Variation in joint stiffness with different stiffness coefficients.

The relationship between external force F_1 applied at the end of the manipulator and moving displacement Δx of the slider is shown in Fig. 9. With an increase in the

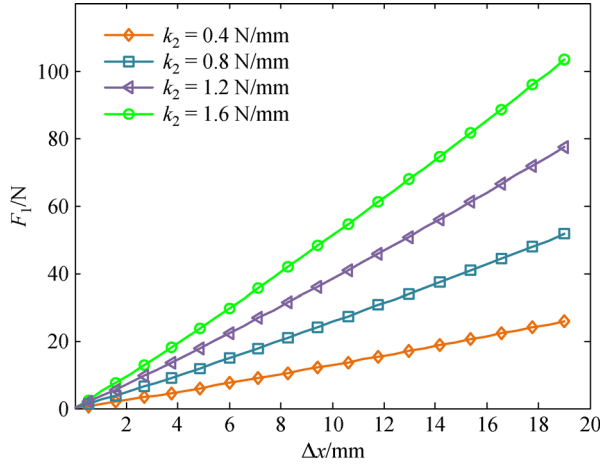


Fig. 9 External force at the end of the arm with different spring stretching.

displacement of the slider, the external force applied to the end of the manipulator increases gradually and is approximately linear.

5 Experimental study

5.1 Prototype development and performance testing

The experimental platform is shown in Fig. 10, and its main parameters of the stiffness-self-adjustable module are shown as follows:

- Stiffness of the torsion spring k_1 : $25 \text{ N} \cdot \text{m}/(^{\circ})$;
- Stiffness of the stretching spring k_2 : $0.8 \text{ N}/\text{mm}$;
- Diameter: 90 mm ;
- Height: 50 mm ;
- Maximum output torque: $20 \text{ N} \cdot \text{m}$;
- Mass: 0.97 kg ;
- Range of change in relative deflection: $[-12^{\circ}, +12^{\circ}]$;

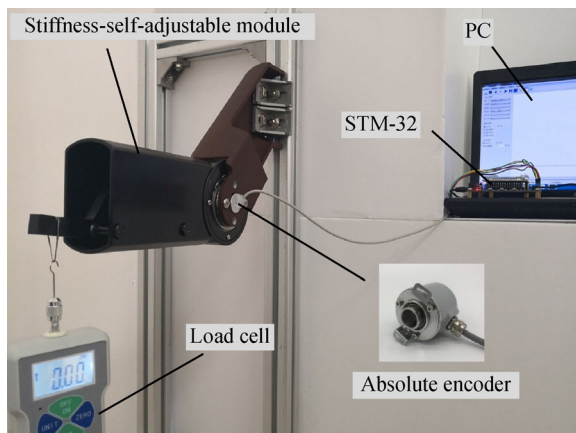


Fig. 10 Experimental platform of the prototype.

Range of stiffness: $[0.51, +\infty) \text{ N} \cdot \text{m}/(^{\circ})$.

The maximum output torque is the product of F_1 and the distance between the force points of F_1 and the rotation center of the joint when the slider moves to the end of the chute.

The stiffness-self-adjustable module is made of aluminum alloy so that the joint's weight can be as small as possible when the design requirements are satisfied. The absolute encoder is composed by a supporting structure and MXAS12-SSI-D2003-V1. The STM32 (STM32H74 3XI6 EVAL BRD) is linked to absolute encoder and PC, where the sampling frequency is set as 50 Hz .

During the stiffness testing, a loading weight is suspended at the end of the arm as the equivalent of external force, and the rotation angle of the elbow joint is measured. The angle of the joint is measured using an absolute encoder fixed to the connecting cover.

A different rotation angle of the joint can be obtained by changing the suspension weight, thereby allowing the attainment of a practical stiffness curve. The experimental curves are fitted by acquiring the average value of the data obtained from five tests. Figure 11 shows a comparison of the theoretical and actual testing stiffness of the stiffness-self-adjustable module versus external force. The diagram indicates that the actual stiffness curve is in good agreement with the theoretical curve in terms of the change trend, and this verifies the functional effectiveness of the proposed stiffness-self-adjustable module. However, a difference remains between the actual measured and theoretical values, and it increases with external force.

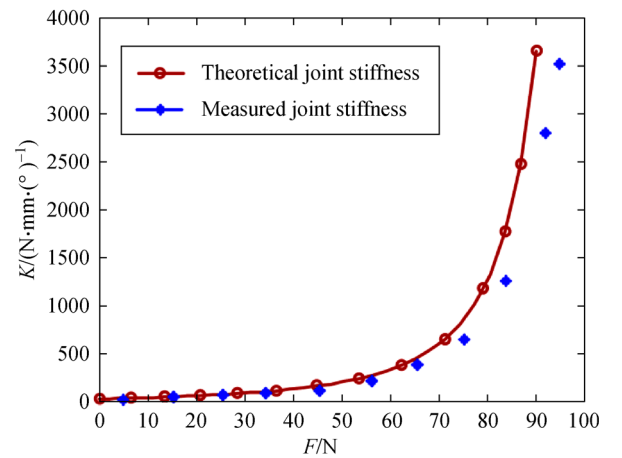


Fig. 11 Validation of the stiffness model of the stiffness-self-adjustable module through experiments.

Under the condition of variable stiffness of $120 \text{ N} \cdot \text{m}/(^{\circ})$, the step response of the position change for loads of 0 and 1 kg is shown in Fig. 12. The time from 0° to 120° is about 75 ms . The results indicate that the response speed of the stiffness adjustment of the mechanical structure is high, and the overshoot time is short.

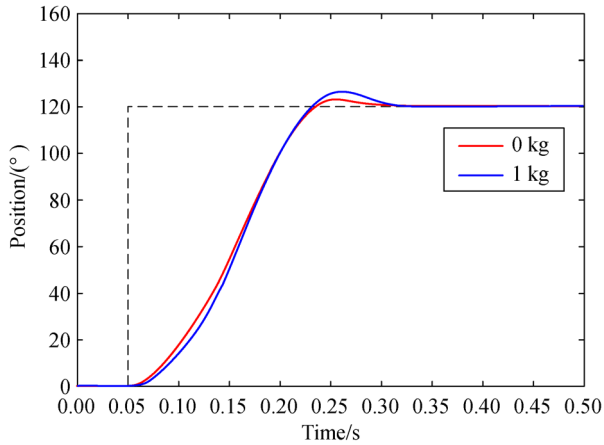


Fig. 12 Step response for the position of the variable stiffness mechanism at loads of 0 and 1 kg.

Figure 13 shows the theoretical stiffness step response at $160 \text{ N}\cdot\text{m}/(^{\circ})$ with an external load 28 N applied to the variable stiffness mechanism. The mechanism reaches the

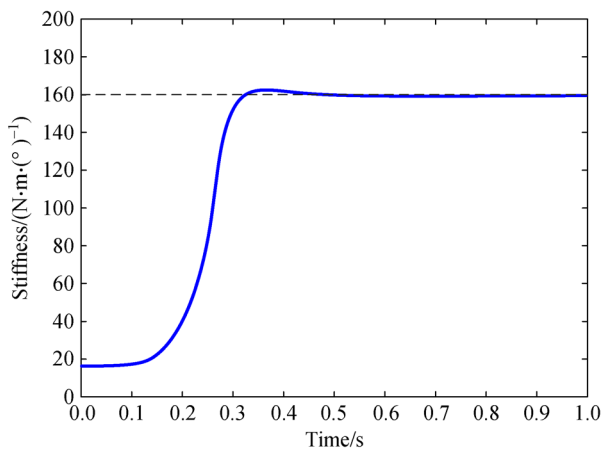


Fig. 13 Step response for the stiffness of the variable stiffness mechanism.

reference value within 500 ms, and the overshoot is small. The stiffness curve of the mechanism in the first half is gentle, but the curve in the second half rises rapidly due to the hysteresis of the torsion spring and synchronous belt.

The static stiffness of the variable stiffness mechanism is examined, as shown in Fig. 14. When no load exists on the end of the regulation module, the stiffness-self-adjustable module is horizontal, and the angle between the end of the regulation module and the side line of the stiffness-self-adjustable module is 83.7° , as shown in Fig. 14(a). When the load of 11.29 N is applied instantaneously, the stiffness-self-adjustable module deflects downward by 7.43° , and the angle between the end of the regulation module and the side line of the stiffness-self-adjustable module is 85.18° , as shown in Fig. 14(b). When the load of 64.13 N is applied instantaneously, the stiffness-self-adjustable module shifts to the horizontal state, and the maximum deformation angle of the regulation module is 96.13° , as shown in Fig. 14(c). These results verify that the variable stiffness mechanism imitates the human arm state.

The regulation module imitates the function of the human wrist, and the stiffness-self-adjustable module imitates the function of the human elbow. When people use their arms to lift objects, the wrist cooperates with the elbow in accordance with the weight of objects, thus making lifting labor-saving. When the weight is small, the wrist angle changes minimally, and the arm bends to a certain angle. When the weight is large, the wrist angle increases, and the muscle-controlled elbow becomes tight and contracts. In the proposed mechanism, the stiffness-self-adjustable module remains horizontal when no load is applied. When a small load is applied, the regulation module moves to the force direction and makes the external force point in the stiffness-self-adjustable module move to the fulcrum. Meanwhile, the synchronous belt rotates, and the energy is stored in the torsion spring. When a large load is applied, the regulation module deflects greatly and pushes the external force action point of the

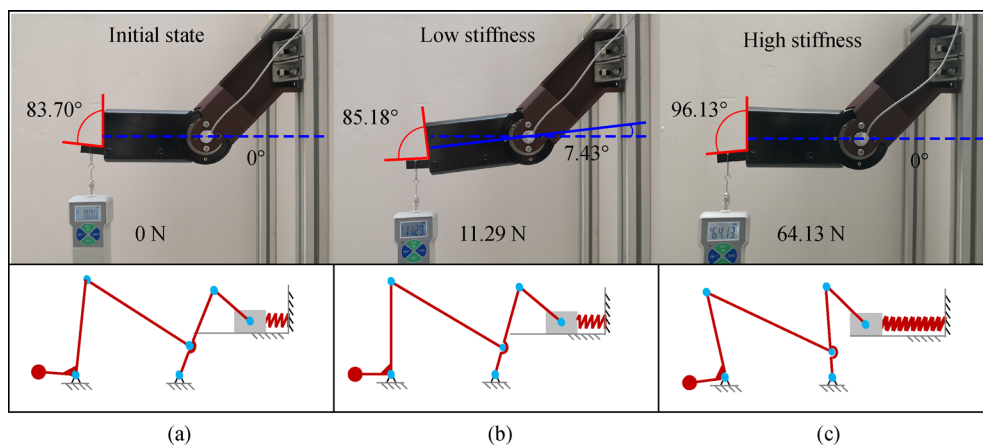


Fig. 14 Status of the variable stiffness mechanism under three situations: External force of (a) 0 N, (b) 11.29 N, and (c) 64.13 N.

stiffness-self-adjustable module to coincide with the fulcrum. As a result, the synchronous belt cannot rotate, and the stiffness-self-adjustable module is almost horizontal.

5.2 Results and discussion

In the proposed design, the adjustment module is used to simulate the state of the human arm when lifting an object; thus, the design can only be subjected to a downward load in a single direction. By replacing other adjustment modules, the stiffness-self-adjustable module can realize stiffness adjustment in two directions.

A noticeable difference still exists between the actual measured value of rigidity and the theoretical value under large external force.

According to the previous design and analysis, the greater the external force applied at the end of the arm is, the greater the distance the external force point moves and the smaller the deflection angle of the joint is. Owing to the limit machining and assembly precision of the parts, particularly the elastic characteristics of the non-metallic synchronous belt, the deflection angle incurs a large error, which creates a discrepancy between the experimental data and the theoretical value.

Two main errors are found in the analysis results. The first one is the displacement error of the external force action point, and the second one is the elastic deformation error of the synchronous belt. Assuming that the deviation in the displacement of the slider is δ , the modified version of the stiffness formula is

$$K_1 = \frac{k_1(x_1 - \delta)^2 R^2}{r^2(\Delta - x_1 - \delta)^2}. \quad (22)$$

Similarly, assuming that the deviation in the angle of the joint is $\Delta\phi$, the modified stiffness formula is

$$K_1 = \frac{k_1(x_1 - \delta)^2 R^2 \phi}{r^2(\Delta - x_1 + \delta)^2(\phi + \Delta\phi)}. \quad (23)$$

Assuming that the elastic deformation of the synchronous belt is Δx when the force is F_0 , the relationship between the elastic deformation Δx of the synchronous belt and the deviation in angle $\Delta\phi$ of the joint can be obtained.

$$\Delta\phi = \frac{\Delta - x_1 + \delta}{(x_1 - \delta)R} \Delta x. \quad (24)$$

The relationship between the elastic deformation Δx of the synchronous belt and external force F_1 at the end of the boom is

$$\Delta x = \frac{3F_1 L(\Delta - x_1 + \delta)}{4R(x_1 - \delta)}. \quad (25)$$

The relationship between the deflection angle and force exerted on the end of the boom can be obtained with

Eqs. (22) and (23).

$$\Delta\phi = \frac{3F_1 L(\Delta - x_1 + \delta)^2}{4R^2(x_1 - \delta)^2}. \quad (26)$$

By substituting deflection angle $\Delta\phi$ into Eq. (21), we derive the following:

$$K_1 = k_1 \frac{(x_1 - \delta)^2 R^2}{r^2(\Delta - x_1 + \delta)^2} \cdot \left(1 - \frac{3F_1 L(\Delta - x_1 + \delta)^2}{4R^2(x_1 - \delta)^2 \phi + 3F_1 L(\Delta - x_1 + \delta)^2} \right). \quad (27)$$

According to the synchronization belt manual, the elongation of the synchronous belt is ≤ 4.0 . The maximum elongation of m is 0.5 here. In addition, the displacement error of the external force action point reaches a maximum value of 1.5 mm. The curve of the joint stiffness can be obtained, as shown in Fig. 15.

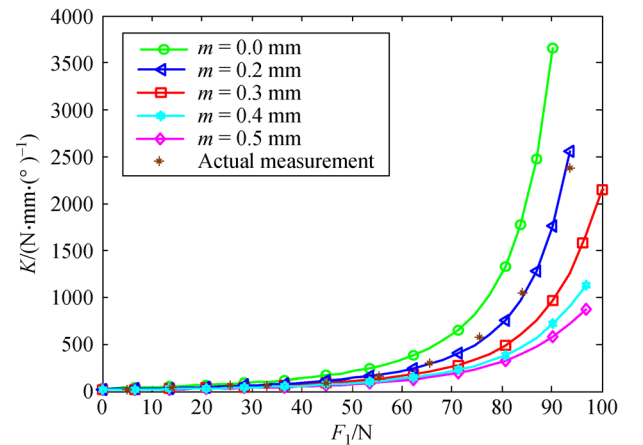


Fig. 15 Interval of stiffness change after correction.

The actual tested stiffness should be greater than the corrected stiffness because the limit value of joint stiffness is used in the correction. However, the theoretical calculation does not consider the influence of error factors, and the theoretical stiffness is greater than the actual tested stiffness. As can be seen from Fig. 15, the curve of the actual tested stiffness is between the theoretical change curve and the correction curve, which verifies the correctness of the theoretical derivation. When the elongation of synchronous belt m is 0.2 mm and the displacement error of the external force action point δ is 0.6 mm, the fitting of the stiffness curve coincides with the actual stiffness change curve.

6 Conclusions

A new passive power-source-free stiffness-self-adjustable

mechanism for the elbow joint of a robot arm was proposed to deal with the problems inherent in current passive stiffness joints. The proposed mechanism does not require a special stiffness regulating motor or sensors and realizes large-range self-adaptive adjustment of stiffness in a purely mechanical manner without the use of sensors or control algorithms. The characteristics of the human arm were simulated in this study, and an optimal arrangement was designed. The weight of the gripped object gripped was taken as information, and the stiffness of the joint was automatically adjusted in accordance with the variation in gravity on the heavy object. The kinematics, statistics, and stiffness model of the stiffness-self-adjustable module were established, and the change trend of joint stiffness under different conditions was obtained. Then, an experimental platform was built, and an experimental study was performed. The results of the experimental test and theoretical calculation were compared and analyzed. The test value was in accordance with the change trend of the theoretical value, and the validity of the proposed passive power-source-free stiffness-self-adjustable mechanism was verified. Furthermore, the test results were influenced by the parts of and elastic change in the synchronous belt, especially when the external force was large. Further analysis revealed that when actual errors and elastic deformation were considered, the actual test values were within the possible theoretical range, thus verifying the correctness of the stiffness theory applied.

Acknowledgements The authors express their gratitude to the referees for carefully reading the paper and providing constructive comments and detailed suggestions for improvement. The authors are also thankful to postgraduate student Qiang Cheng for his support during the writing of the paper. This study was supported by the National Key R&D Program of China (Grant No. 2018YFB1304600), the National Natural Science Foundation of China (Grant Nos. 51975566 and 61821005), and the CAS Interdisciplinary Innovation Team (Grant No. JCTD-2018-11).

Open Access This article is licensed under a Creative Commons Attribution 4.0 International License, which permits use, sharing, adaptation, distribution and reproduction in any medium or format, as long as you give appropriate credit to the original author(s) and the source, provide a link to the Creative Commons licence, and indicate if changes were made.

The images or other third party material in this article are included in the article's Creative Commons licence, unless indicated otherwise in a credit line to the material. If material is not included in the article's Creative Commons licence and your intended use is not permitted by statutory regulation or exceeds the permitted use, you will need to obtain permission directly from the copyright holder.

To view a copy of this licence, visit <http://creativecommons.org/licenses/by/4.0/>.

References

1. Ding H, Yang X, Zheng N, et al. Tri-co robot: A Chinese robotic research initiative for enhanced robot interaction capabilities. *National Science Review*, 2018, 5(6): 799–801
2. Hirzinger G, Bals J, Otter M, et al. The DLR-KUKA success story: Robotics research improves industrial robots. *IEEE Robotics & Automation Magazine*, 2005, 12(3): 16–23
3. Ham V R, Sugar T G, Vanderborght B, et al. Compliant actuator designs: Review of actuators with passive adjustable compliance/controllable stiffness for robotic applications. *IEEE Robotics & Automation Magazine*, 2009, 16(3): 81–94
4. Vanderborght B, Albu-Schaeffer A, Bicchi A, et al. Variable impedance actuators: A review. *Robotics and Autonomous Systems*, 2013, 61(12): 1601–1614
5. Tagliamonte N L, Sergi F, Accoto D, et al. Double actuation architectures for rendering variable impedance in compliant robots: A review. *Mechatronics*, 2012, 22(8): 1187–1203
6. Wolf S, Grioli G, Eiberger O, et al. Variable stiffness actuators: Review on design and components. *IEEE/ASME Transactions on Mechatronics*, 2016, 21(5): 2418–2430
7. Pratt G A, Williamson M M. Series elastic actuators. In: *Proceedings of International Conference on Intelligent Robots and Systems. Human Robot Interaction and Cooperative Robots*. Pittsburgh: IEEE, 1995, 399
8. Wolf S, Eiberger O, Hirzinger G. The DLR FSJ: Energy based design of a variable stiffness joint. In: *Proceedings of IEEE International Conference on Robotics and Automation*. Shanghai: IEEE, 2011, 5082–5089
9. Jafari A, Tsagarakis N, Caldwell D. Energy efficient actuators with adjustable stiffness: A review on AwAS, AwAS-II and CompACT VSA changing stiffness based on lever mechanism. *Industrial Robot*, 2015, 42(3): 242–251
10. Yigit C B, Bayraktar E, Boyraz P. Low-cost variable stiffness joint design using translational variable radius pulleys. *Mechanism and Machine Theory*, 2018, 130: 203–219
11. Edsinger A L. Robot manipulation in human environments. Dissertation for the Doctoral Degree. Boston: Massachusetts Institute of Technology, 2007, 102–109
12. Morita T, Iwata H, Sugano S. Development of human symbiotic robot: WENDY. In: *Proceedings of IEEE International Conference on Robotics and Automation*. Detroit: IEEE, 1999, 3183–3188
13. Tsagarakis N G, Li Z, Saglia J. The design of the lower body of the compliant humanoid robot ‘cCub’. In: *Proceedings of IEEE International Conference on Robotics and Automation*. Shanghai: IEEE, 2011, 2035–2040
14. Malosio M, Spagnuolo G, Prini A, et al. Principle of operation of RotWWC-VSA, a multi-turn rotational variable stiffness actuator. *Mechanism and Machine Theory*, 2017, 116: 34–49
15. Hurst J W, Chestnutt J E, Rizzi A A. The actuator with mechanically adjustable series compliance. *IEEE Transactions on Robotics*, 2010, 26(4): 597–606
16. Eiberger O, Haddadin S, Weis M. On joint design with intrinsic variable compliance: Derivation of the DLR QA-Joint. In: *Proceedings of IEEE International Conference on Robotics and Automation*. Anchorage: IEEE, 2010, 1687–1694
17. Friedl W, Höppner H, Petit F. Wrist and forearm rotation of the DLR Hand Arm System: Mechanical design, shape analysis and experimental validation. In: *Proceedings of International Conference on Intelligent Robots and Systems*. San Francisco: IEEE, 2011, 1836–1842
18. Wolf S, Hirzinger G. A new variable stiffness design: Matching

- requirements of the next robot generation. In: Proceedings of IEEE International Conference on Robotics and Automation. Pasadena: IEEE, 2008, 1741–1746
19. Jafari A, Tsagarakis N G, Sardellitti I, et al. A new actuator with adjustable stiffness based on a variable ratio lever mechanism. *IEEE/ASME Transactions on Mechatronics*, 2014, 19(1): 55–63
 20. Kim B S, Song J B. Design and control of a variable stiffness actuator based on adjustable moment arm. *IEEE Transactions on Robotics*, 2015, 28(5): 1145–1151
 21. Groothuis S S, Rusticelli G, Zucchelli A, et al. The variable stiffness actuator vsaUT-II: Mechanical design, modeling, and identification. *IEEE/ASME Transactions on Mechatronics*, 2014, 19(2): 589–597
 22. Van Ham R, Vanderborght B, Van Damme M, et al. MACCEPA, the mechanically adjustable compliance and controllable equilibrium position actuator: Design and implementation in a biped robot. *Robotics and Autonomous Systems*, 2007, 55(10): 761–768
 23. Vanderborght B, Tsagarakis N G, Semini C, et al. MACCEPA 2.0: Adjustable compliant actuator with stiffening characteristic for energy efficient hopping. In: Proceedings of International Conference on Robotics and Automation. Kobe: IEEE, 2009, 544–549
 24. Fang L, Wang Y. Study on the stiffness property of a variable stiffness joint using a leaf spring. *Proceedings of the Institution of Mechanical Engineers, Part C: Journal of Mechanical Engineering Science*, 2018, 1989–1996: 203–210
 25. Bi S S, Liu C, Zhao H Z, et al. Design and analysis of a novel variable stiffness actuator based on parallel-assembled-folded serial leaf springs. *Advanced Robotics*, 2017, 31(18): 990–1001
 26. Liu L, Leonhardt S, Misgeld B J E. Design and control of a mechanical rotary variable impedance actuator. *Mechatronics*, 2016, 39: 226–236
 27. Wang W, Fu X, Li Y, et al. Design of variable stiffness actuator based on modified gear-rack mechanism. *Journal of Mechanisms and Robotics*, 2016, 8(6): 061008
 28. Choi J, Hong S, Lee W, et al. A robot joint with variable stiffness using leaf springs. *IEEE Transactions on Robotics*, 2011, 27(2): 229–238
 29. Tao Y, Wang T, Wang Y, et al. Design and modeling of a new variable stiffness robot joint. In: Proceedings of 2014 International Conference on Multisensor Fusion and Information Integration for Intelligent Systems (MFI). Beijing: IEEE, 2015
 30. Liu Y, Liu X, Yuan Z, et al. Design and analysis of spring parallel variable stiffness actuator based on antagonistic principle. *Mechanism and Machine Theory*, 2019, 140: 44–58
 31. Shadmehr R, Arbib M A. A mathematical analysis of the force-stiffness characteristics of muscles in control of a single joint system. *Biological Cybernetics*, 1992, 66(6): 463–477
 32. Chang H, Kim S J, Kim J. Feedforward motion control with a variable stiffness actuator inspired by muscle cross-bridge kinematics. *IEEE Transactions on Robotics*, 2019, 35(3): 747–760
 33. Mata A S, Torras A B, Carrillo J A C. *Fundamentals of Machine Theory and Mechanisms*. Cham: Springer, 2016